Articles

Transition State Model and Mechanism of Nucleophilic Aromatic Substitution Reactions Catalyzed by Human Glutathione *S*-Transferase M1a-1a[†]

Yury Patskovsky, Larysa Patskovska, Steven C. Almo, and Irving Listowsky*

Department of Biochemistry, Albert Einstein College of Medicine, Bronx, New York 10461

Received September 9, 2005; Revised Manuscript Received February 6, 2006

ABSTRACT: An active site His107 residue distinguishes human glutathione *S*-transferase hGSTM1-1 from other mammalian Mu-class GSTs. The crystal structure of hGSTM1a-1a with bound glutathione (GSH) was solved to 1.9 Å resolution, and site-directed mutagenesis supports the conclusion that a proton transfer occurs in which bound water at the catalytic site acts as a primary proton acceptor from the GSH thiol group to transfer the proton to His107. The structure of the second substrate-binding site (H-site) was determined from hGSTM1a-1a complexed with 1-glutathionyl-2,4-dinitrobenzene (GS-DNB) formed by a reaction in the crystal between GSH and 1-chloro-2,4-dinitrobenzene (CDNB). In that structure, the GSH-binding site (G-site) is occupied by the GSH moiety of the product in the same configuration as that of the enzyme−GSH complex, and the dinitrobenzene ring is anchored between the side chains of Tyr6, Leu12, His107, Met108, and Tyr115. This orientation suggested a distinct transition state that was substantiated from the structure of hGSTM1a-1a complexed with transition state analogue 1-*S*-(glutathionyl)-2,4,6-trinitrocyclohexadienate (Meisenheimer complex). Kinetic data for GSTM1a-1a indicate that $k_{cat}^{(CDNB)}$ for the reaction is more than 3 times greater than $k_{cat}^{(FDNB)}$, even though the nonenzymatic second-order rate constant is more than 50-fold greater for 1-fluoro-2,4-dinitrobenzene (FDNB), and the product is the same for both substrates. In addition, $K_m^{(FDNB)}$ is about 20 times less than $K_m^{(CDNB)}$. The results are consistent with a mechanism in which the formation of the transition state is rate-limiting in the nucleophilic aromatic substitution reactions. Data obtained with active-site mutants support transition states in which Tyr115, Tyr6, and His107 side chains are involved in the stabilization of the Meisenheimer complex via interactions with the ortho nitro group of CDNB or FDNB and provide insight into the means by which GSTs adapt to accommodate different substrates.

Glutathione *S*-transferases (GSTs)[1] catalyze nucleophilic addition and substitution reactions utilizing GSH to detoxify a wide variety of electrophilic substrates (*1*−*10*). Mammalian GSTs are products of gene superfamilies, and multiple forms within a class are thought to originate from gene duplication or conversion events (*5*, *7*, *11*−*13*). Species-independent classification and nomenclature systems have been devised on the basis of common properties (*7*, *14*−*16*). Subunit types from within each class, but not between classes, assemble in homo or heterodimeric combinations. Human GSTs exhibit discrete genetic polymorphisms, the most notable of which is a deletion of the *hGSTM1* gene in approximately 50% of the population (*12*, *17*−*19*), which has been correlated with individual variations in susceptibility to some cancers and to differences in response to drugs(*20*). There are five homologous human Mu-class GST subunit types, four of which (hGSTM1, hGSTM2, hGSTM4, and hGSTM5) represent natural structural variants with extensive regions of sequence identity (*18*, *21*). hGSTM1-1 is also unique among the Mu-class GSTs from a structural standpoint owing to the presence of His107 in the catalytic pocket, whereas most other human and rodent GSTs have an arginine at that position. Previous mechanistic and mutagenesis studies suggested that His107 of hGSTM1a-1a, which is located near the active site pocket, acts as a general base by lowering the p*K* value of enzyme-bound GSH (*22*).

A structural basis of enzymatic activity has been proposed for other members of Mu-class GSTs including human hGSTM2-2 (*23*), which contains Arg107 residues. Rat GSTM1-1 (rGSTM1-1)(*24*) and hGSTM2-2 (*25*) have been crystallized in the presence of GSH, GS-DNB (*26*), potential transition-state complexes (rat rGSTM1-1, pdb 5GST), or ligand-free forms. Two substrate-binding sites have been delineated: the GSH-binding site (G-site) and the second substrate-binding site for hydrophobic compounds (H-site) (*14*, *27*, *28*). For all Mu-class GSTs, the G-site is composed

[†] This work was supported by grants CA-42448 and GM-62529 from the National Institutes of Health.

* To whom correspondence should be addressed. Tel: 718-430-2276. Fax: 718-430-8565. E-mail: irving@aecom.yu.edu.

[1] Abbreviations: GSH, glutathione; GST, glutathione *S*-transferase; CDNB, 1-chloro-2,4-dinitrobenzene; FDNB, 1-fluoro-2,4-dinitrobenzene, GS-DNB, 1-*S*-glutathionyl-2,4-dinitrobenzene; Meisenheimer complex, 1-*S*-(glutathionyl)-2,4,6-trinitrocyclohexadienate; TNB, 1,3,5-tri(nitro)benzene.

10.1021/bi051823+ CCC: $33.50
Published on Web 03/01/2006

of invariant residues, and the G-site topology appears to be strictly conserved. The H-site residues are less conserved among members of the Mu family, providing a basis for overlapping yet different substrate specificities among the Mu-class enzymes (*8*, *29*).

In this article, the high-resolution crystal structures of hGSTM1a-1a complexed with GSH, GS-DNB, and transition state analogue 1-*S*-(glutathionyl)-2,4,6-trinitrocyclohexadienate were solved, and the amino acid residues potentially involved in catalysis were identified and mutated, and the kinetic parameters of the mutant enzymes with CDNB and FDNB as second substrates were analyzed. A transition state model is proposed and a mechanism is presented in which the chemistry for the formation of the transition state probably is rate limiting for nucleophilic aromatic substitution reactions catalyzed by hGSTM1a-1a.

MATERIALS AND METHODS

Protein Expression and Purification. Human GSTM1a-1a was cloned and expressed in *E. coli* BL21 (DE3) using the *pET3a* expression vector as previously described (*22*). Site-directed mutagenesis was performed using PCR and a set of specific oligonucleotide primers as described(*22*). The amino acid sequence of each mutant protein was verified by mass spectrometry (*30*). Wild-type and mutant enzymes were purified using GSH−agarose (Sigma-Aldrich, St Louis, MO) as an affinity matrix and extensively dialyzed against a 10 mM sodium phosphate buffer (pH 6.5) with 1 mM DTT. Protein solutions were concentrated to about 20−25 mg/mL using 10 and 30K centrifugal Amicon concentrators (Millipore), aliquoted and stored at −70 °C until use. Protein concentrations were determined spectrophotometrically on the basis of absorbance values at 280 nm.

Enzyme Kinetics. 1-Chloro-2,4-dinitrobenzene (CDNB), 1-Fluoro-2,4-dinitrobenzene (FDNB), 1,3,5-trinitrobenzene (TNB), and reduced glutathione (GSH) were purchased from Sigma-Aldrich. Kinetic studies were performed in a 50 mM sodium phosphate buffer. pH Dependence studies were performed over a range of 5.7−9.0 at increments of 0.2 pH units. To determine kinetic constants for GSH and second substrates, the concentration of one substrate was kept constant while the other one was varied at five different concentrations. With CDNB as a second substrate (*31*), the concentration was varied from 10 μM to 2 mM with GSH concentration usually fixed at 2 mM. For most mutants, the same k_{cat} limiting values were also obtained at 0.5 mM GSH concentration. However, with FDNB as a second substrate (*32*, *33*), the nonenzymatic background rates were much greater; thus for technical reasons, lower substrate concentrations were usually employed with 0.2 or 0.5 mM GSH, and the concentration of FDNB was varied between 0.005 and 0.5 mM. Under those conditions, no covalent modifications of the protein were detected by mass spectrometry (ESI MS). The reaction rate was measured spectrophotometrically as described (*22*). All experiments were performed in triplicate and values of the kinetic constants (K_m and k_{cat}) were calculated using SIMFIT software. Because the rate of catalysis is pH dependent, limiting (maximal) values for kinetic constants were calculated for each substrate using plots of k_{cat} versus pH and K_m versus pH as previously described (*22*). The values of kinetic constants k_{obs} of nonenzymatic reactions were determined in the absence of any enzyme using the buffers mentioned above.

Protein Crystallization. Crystallization experiments were performed using hanging or sitting drop-vapor diffusion methods. In brief, 2 μL of hGSTM1a-1a (25 mg/mL or 1mM binding sites) in the presence of 2.0 mM GSH was mixed with an equal volume of precipitant (50 mM sodium phosphate at pH 6.5, 18−22% PEG4000, and 20% glycerol) and equilibrated against 1 mL of the same buffer at +4 °C for 2−6 days. Crystals usually appeared on the second day and continued to grow for 3−4 days until their maximal dimensions reached $0.3 \times 0.5 \times 0.5$ mm^3. The crystals were soaked in mother liquor containing 2 mM GSH and frozen in liquid nitrogen before data collection. The best crystal diffracted to 1.9 Å with a mosaicity of approximately 0.6°.

Solid-State Catalysis. To obtain the hGSTM1−GS-DNB complex, crystals of hGSTM1a-1a grown in the presence of 2 mM GSH and 20% glycerol were soaked in crystallization buffer A (50 mM sodium phosphate at pH 6.0, 25% PEG4000, 20% glycerol, and 2 mM GSH) containing 2.0 mM CDNB as follows: first, 0.2 μL of concentrated CDNB (40 mM) solution in pure ethanol was applied on a clean cover slip and allowed to evaporate to dryness. Subsequently, 4 μL of crystallization buffer A was added to the same spot and mixed carefully to form a uniform suspension. (CDNB is much less soluble in water than in alcohols.) The protein crystal was then transferred to the drop, which was quickly sealed (to avoid evaporation), and allowed to equilibrate against crystallization buffer A. In 1−2 min, the drop and the crystal together became yellow in color (GS-DNB is a yellow colored product), and the colorless precipitate (CDNB) disappeared. The crystal was incubated for an additional 30 min, flash frozen as described above, and used for X-ray data collection. After transferring the protein crystals to the drop containing CDNB, the crystals remained visually stable and within a few seconds started to develop a yellow color. (These observations do not constitute direct proof that solid-state catalysis occurs in solution in the same way.) At that time, the solution remained with no visible color, and the first signs of yellow color appeared only around the crystals.

To obtain the hGSTM1a-a complexed with 1-*S*-(glutathionyl)-2,4,6-trinitrocyclohexadienate (transition state analogue), the crystals of hGSTM1a-1a were incubated in the mother liquor in the presence of 2.0 mM TNB and 2.0 mM GSH as described above for the GS-DNB complex. After 1−2 min of incubation, the protein crystals started to develop a reddish color, and after 8−10 min of incubation, the crystals were frozen and used for X-ray data collection. The solution surrounding the crystals remained colorless even after prolonged (up to 24 h) incubation.

X-ray Data Collection, Structure Solution, and Refinement. X-ray data were collected under cryogenic conditions using a Rigaku RU-200 X-ray generator coupled to a RIGAKU R-AXIS IV image plate. Data were reduced and scaled with DENZO and SCALEPACK. The structures were solved by molecular replacement using coordinates for monomer A of ligand-free hGSTM1a-1a (1GTU) as a starting model and *MOLREP* software (*CCP4* program suit). Each model was initially refined by *REFMAC5* (*CCP4* program suit) and subsequently simulated annealing (slow cooling), positional, and isotropic *B* factor refinement using *X-PLOR* (version 8.851) and *CNS* (version 1.0) (*34*, *35*). Models were corrected

manually using O and TOM software. When R_{free} values dropped below 28% for each structure, the ligands were fitted manually using Fo-Fc and 2Fo-Fc electron density maps. Topological and parametrical files for GSH and GS-DNB were created using *XPLO2D* (*36*) and corrected manually. After additional rounds of positional refinement, R_{free} values dropped below 27%. Water molecules were added automatically (*X-PLOR*) to each model using 2Fo-Fc electron density maps, and their positions were refined manually in programs O and TOM. The stereochemistry of the models was verified by *PROCHECK* (*37*). Molecular modeling was performed using INSIGHTII (Accelrys Inc.) software.

RESULTS

Structural Aspects of the hGSTM1a-1a−GSH Binary Complex. hGSTM1a-1a is composed of two identical subunits that are related by a C2 2-fold symmetry axis. The overall 3D structure of the GSH−enzyme complex (pdb 1XW6) is very similar to that of the ligand-free enzyme (pdb 1GTU) (*22*). The root-mean-square difference (RMSD) between the coordinates of the Cα atoms of the monomers for those two structures does not exceed 0.35 Å. Because the structure for the ligand-free hGSTM1-1a (1GTU) was solved at a lower resolution (2.7 Å) than that of the GSH−enzyme complex reported here (1.9 Å), some additional structural details that were not represented in the ligand-free structure became evident. For instance, the residues of the flexible μ-loop are usually poorly defined in electron density (ED) maps previously reported for hGSTM2-2 and rGSTM1-1 (*24*, *38*). However, in the structure of the hGSTM1a-1a−GSH complex, the μ-loop is very well resolved in ED maps even though this part of the molecule still appears flexible with *B* factors ranging from 35 to 50 Å^2. (The average *B* factor for all atoms of the model is 36.10 Å^2). A key residue of the μ-loop is the *cis*-Pro38, which was previously assigned a trans configuration in the structure 1GTU and in the coordinate files for hGSTM2-2 (pdb 1NHA). Thus, three proline residues of each hGSTM1a subunit are in the cis configuration: Pro38 of the μ-loop, Pro60, which is a part of the G-site, and Pro206, located near the *C*-terminus and close to the H-site. There are two allelic variants of hGSTM1, Lys172 (M1a), and Asn172 (M1b), but no significant phenotypic differences have been associated with these variants so far. In the 3D structure, residue 172 is located at the protein surface, far from the active sites or the dimer interface and may thus represent an example of a silent mutation. The overall 3D structure of each monomer of the homodimer of the binary complex is essentially the same as that of the ligand-free form; GSH binding does not result in significant structural changes. The RMSD between GSH-bound and ligand-free homodimers is 0.42 Å.

Catalytic G-Site Topology. The 2Fo-Fc electron density map for the key residues of the G-site is shown in Figure 1A. The G-site appears as a rigid part of the protein, the side chains of the G-site residues (with the exception of Met108) retain their orientations, and the overall protein structure remains essentially unchanged upon GSH binding. The two water molecules shown in Figure 1A align to the sulfur atom of GSH and the His107 side chain. Although the imidazole side chain of His107 bears two potential hydrogen bond donors, no direct polar interactions with any other protein atoms were evident. One water molecule connects the Nδ atom of the His107 imidazole group, the carboxyl group of Asp161, and the backbone carbonyl oxygen of Leu158 (not shown in the Figure). The Nξ atom of the His107 side chain is probably hydrogen bonded to the water molecule designated as WAT2 in Figure 1, and WAT2 is also hydrogen bonded to a second water molecule (WAT1) which is about 3.2 Å away from the sulfur atom of GSH and could be hydrogen bonded to the hydroxyl groups of Tyr115 and Tyr6. These water molecules are well defined in electron density (ED) maps with *B* factor values ranging from 20 to about 40 Å^2, which are similar to those of neighboring amino acid side chains.

The Tyr115 and Tyr6 side chains are also involved in polar intrasubunit interactions. For instance, the side chain Tyr6 hydroxyl group is a hydrogen bond acceptor for the backbone amide group of Leu12. Apart from that, a proton is likely shared by the GSH-thiolate anion and the Tyr6 hydroxyl group. In this case, Tyr6 serves as a hydrogen bond donor, and the thiolate anion may be considered to be a hydrogen bond acceptor. The Tyr115 hydroxyl group is hydrogen bonded to the backbone amide of Ser209. Additional water molecules are associated with WAT2 and the sulfur atom of GSH. WAT1 and WAT2 are located within the H-site and are replaced by a second substrate during catalysis.

GSH binds to the G-site by displacing water molecules present in the ligand-free enzyme. The bound tripeptide is stabilized by numerous polar and nonpolar interactions involving protein atoms and solvent molecules. The α-carboxyl group of GSH is hydrogen bonded to the side chain hydroxyl and backbone amide groups of Ser72. The α-carboxyl group is also hydrogen bonded to a water molecule, which in turn connects the backbone carbonyl of Pro60 to the backbone amide of Asn71. Another water molecule is within hydrogen bond distance of the α- carboxyl group of GSH, the backbone amide of Asn73, the side chain carbonyl oxygen of Gln71, and the side chain hydroxyl group of Ser72. The γ-Glu amino moiety of GSH is likely to be hydrogen bonded to the carbonyl oxygen of the Gln71 side chain, to the carboxyl group of the Asp105 side chain, which is from the other subunit of the dimer, and to a water molecule. The water molecule is located within hydrogen bond distance from the sulfur atoms of Met104 and Met108, suggesting indirect involvement of those residues as well in GSH binding. Moreover, the Met108 side chain changes its relative orientation after GSH binding, and the mutagenesis of each of these two methionine residues causes a moderate yet detectable effect on GSH, second substrate K_m values, and catalytic rates (see below). Other than that, the G-site topology is sufficiently rigid to retain its conformation in the absence of GSH. The Arg42, Trp45, and Asn58 side chains and the backbone carbonyl oxygen of Leu59 interact with various polar groups of GSH. In addition, the backbone carbonyl oxygen of the cysteine and the *C*-terminal carboxyl group of the glycine residue of GSH are solvated by water molecules.

Crystal Structure of the hGSTM1a-1a−GS-DNB Product Complex. GS-DNB is the product of conjugation reactions between GSH and CDNB or FDNB. To produce an enzyme−product complex, crystals of hGSTM1a-1a grown in the presence of GSH were soaked in a solution containing CDNB. The formation of the product was detected visually

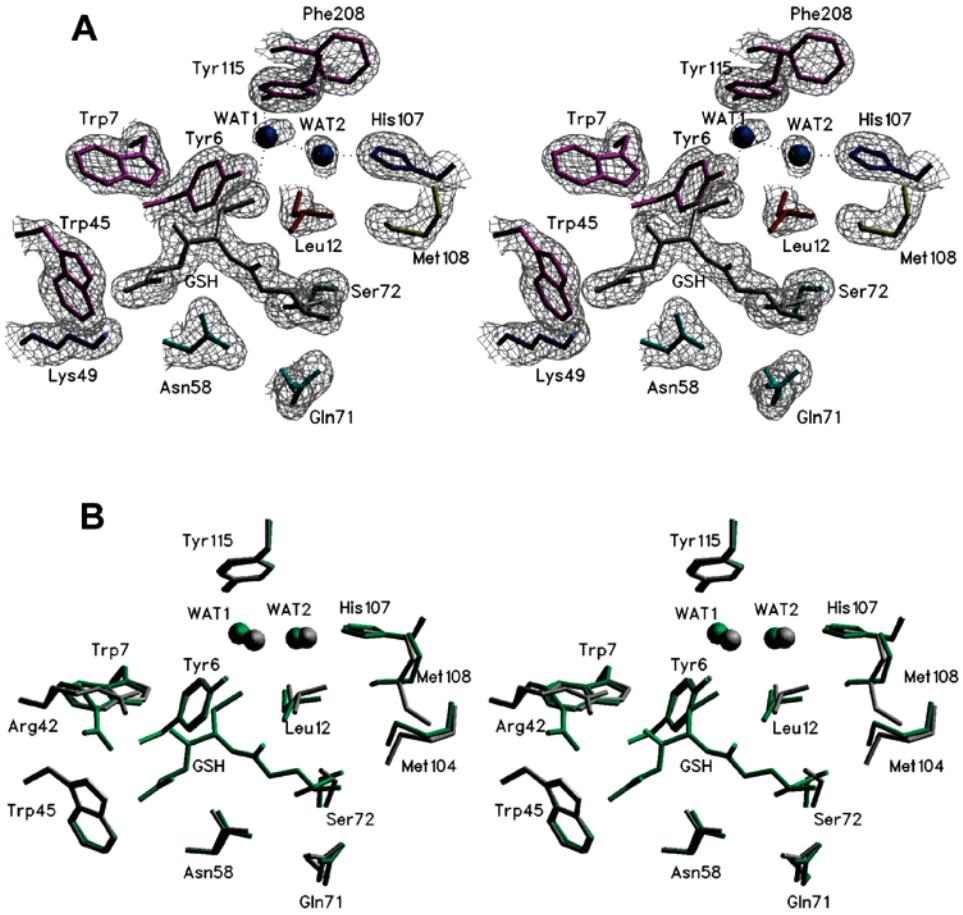

FIGURE 1: Structure of the G-site of human GSTM1a-1a with bound GSH. (A) Stereoview of the 2Fo-Fc omit map (sigma level cutoff 1.0) for residues of the catalytically active site of human GSTM1a-1a complexed with GSH (pdb 1WX6). GSH and water molecules were omitted from map calculations. Putative hydrogen bonds are represented by dotted lines. (B) Stereoview of the superimposition of active-site residues taken from the coordinates of ligand-free (pdb 1GTU, gray) and GSH-complexed (pdb 1WX6, green) hGSTM1a-1a. The coordinates for monomer A were used in each case.

and spectrophotometrically (Materials and Methods), suggesting that the crystallized form of the enzyme is catalytically active. Bound GS-DNB is very well defined in the 2Fo-Fc electron density map (Figure 2A) which allows for the detailed analysis of interactions between the ligand, protein atoms, and tightly associated solvent molecules. Superimposition of the GSH-enzyme and GS-DNB−enzyme complexes is presented in Figure 2B. The RMSD value between the coordinates of the backbone atoms of the homodimers of these two structures (0.41 Å) is close to the value of the estimated coordinate error (0.35 Å for the structure hGSTM1-1(GS-DNB)). The overall configuration of the GSH moiety of GS-DNB is very similar to that of GSH in the GSH−enzyme complex (Figure 1A) with an RMSD value between their atomic coordinates of about 0.3 Å (Figure 2B). These data also support the premise that the G-site is a rigid part of the structure.

The sulfur atom of GS-DNB is located within 4 Å of the hydroxyl oxygen of Tyr6, which is further than the distance between the sulfur atom of GSH and the same Tyr6 oxygen atom (3.2−3.5 Å) in the enzyme−GSH complex. It is noteworthy that the oxygen atom of the ortho nitro group of GS-DNB is about 4 Å from the hydroxyl group of the Tyr6 side chain, which is far too distant to form a productive hydrogen bond. However, this observation represents the first clear structural indication that Tyr6 can be involved in catalysis either by the binding of the second substrate or by stabilizing a transition state complex. Structural data and kinetic studies of GSTM1a-1a mutants provided below support the latter notion.

An analysis of the interactions within the active site of the GS-DNB−GSTM1a-1a complex shows the involvement of polar and nonpolar protein groups as well as solvent molecules in product binding. The ortho nitro group of the dinitrobenzene (DNB) ring is located within hydrogen bonding distance from the Nξ atom of the His107 side chain and from the sulfur atom of the Met108 side chain. A water molecule in the same position as that in the GSH−enzyme complex, connects the side chains of His107 and Asp161 and the backbone carbonyl oxygen of Leu158. Therefore, the Nδ atom of His107 likely remains protonated upon ligand binding. The DNB ring is situated about 3.8−4.0 Å away from the Tyr115 planar aromatic ring, and these two aromatic rings overlap but do not form a typical stacking pair because they are not parallel to each other in the complex (Figure 2). One oxygen atom of the para nitro group is located within 3 Å from the backbone carbonyl oxygen of Gly111, and repulsion rather than favorable interactions between the para nitro group of GS-DNB and the backbone carbonyl oxygen of Gly111 are expected. It is noteworthy that the Gly111 residue in the pocket of hGSTM1a-1a is replaced by bulkier side chains in some other Mu-class GSTs that could affect catalysis. The para nitro group of GS-DNB lies in the same plane as that of the DNB ring, but the ortho nitro group

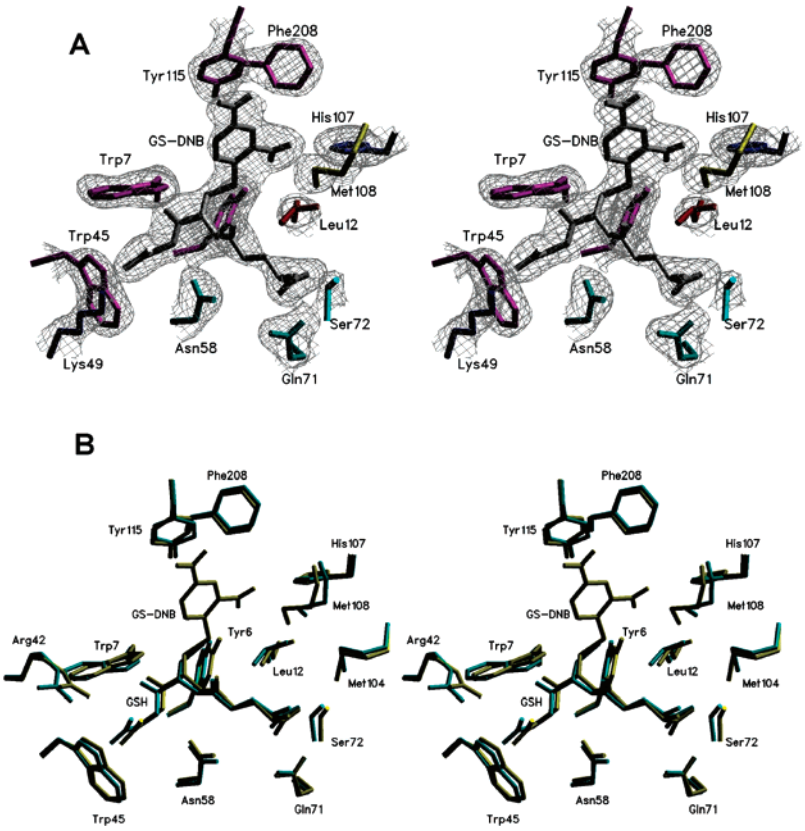

FIGURE 2: Structure of the hGSTM1a−GS-DNB complex. (A) Stereoview of the 2Fo-Fc omit map drawn around residues of the catalytic site of human GSTM1a-1a complexed with GS-DNB (pdb 1WX6). The ligand was omitted from map calculations. (B) Stereoview of the superimposition of active-site residues taken from the coordinates of hGSTM1a-1a complexed with GSH (pdb 1WX6, blue) and GS-DNB (pdb 1WXK, yellow). The coordinates for monomer A were used in each case.

deviates from planarity and is rotated at about a 30° angle with respect to the plane of the DNB ring. The DNB ring displaces water molecules from the active site. Water molecules that are coordinated near the DNB ring of GS-DNB join the backbone carbonyl group of the cysteine residue of GSH, the sulfur atom of the Met108 side chain, and the nitro groups of the ligand, thereby closing the external wall of the H-site of hGSTM1a-1a.

Structure of hGSTM1a-1a Complexed with a Transition State Analogue (1-S-(Glutathionyl)-2,4,6-trinitrocyclohexadienate). Crystals of hGSTM1a-1a soaked in a crystallization solution containing GSH and TNB rapidly developed a reddish color indicating that the reaction produced the product 1-*S*-(glutathionyl)-2,4,6-trinitrocyclohexadienate. The colored product did not diffuse from the crystals suggesting that 1-*S*-(glutathionyl)-2,4,6-trinitrocyclohexadienate has a high affinity to the enzyme. The space group of the crystals changed from *C*2 to *P*1. The changes in lattice contacts did not result in any significant changes in protein tertiary or quaternary structures (pdb 2F3M), and RMSD values between the coordinates of all the atoms of all three structures (hGSTM1a-1a complexed with GSH, GS-DNB, and 1-*S*-(glutathionyl)-2,4,6-trinitrocyclohexadienate) did not exceed 0.45 Å. All side chains within the active site in the structure of hGSTM1a−1-*S*-(glutathionyl)-2,4,6-trinitrocyclohexadienate (with the exception of Met108) retained the same positions as those in the protein−GSH complex. The 2Fo-Fc ED map drawn around active-site residues and 1-*S*-(glutathionyl)-2,4,6-trinitrocyclohexadienate is shown in Figure 3A. The GSH moiety of the ligand is clear in this structure and occupies the G-site of the enzyme with an overall conformation similar to that of GSH in the enzyme−GSH complex (pdb 1XW6). The 2,4,6-trinitrocyclohexadienate moiety of the ligand is linked to GSH (sigma complex). The oxygen atoms of the 2-nitro group of 2,4,6-trinitrocyclohexadienate are within hydrogen bond distance from the Tyr115 hydroxyl group and the His107 side chain. The Tyr6 hydroxyl group is located about 3.4−3.6 Å from the 2- nitro group of the 2,4,6-trinitrocyclohexadienate moiety, suggesting that this nitro group can be hydrogen bonded to Tyr6. The 4-nitro group of the 2,4,6-trinitrocyclohexadienate ring is located within hydrogen bond distance from the Met108 side chain. No other direct polar interaction between the trinitrocyclohexadienate moiety and the protein atoms was detected. The structure of hGSTM1a-1a complexed with the product GS-DNB is compared with that of the sigma complex in Figure 3B to illustrate the reorientation of the ring after the reaction.

Comparisons with Other Mu-Class GSTs. Crystal structures of GSTs complexed with GS-DNB, the product of the conjugation reaction between GSH and CDNB, have been obtained for rGSTM1-1 (*38*) and hGSTM2-2 (*25*). The DNB ring of the hGSTM1a-1a−GS-DNB complex, produced by soaking the substrates into the crystal in this study, is oriented into the active site, is well defined in ED maps, and shows clear contacts with neighboring amino acid side chains and water. The stereochemistry of GS-DNB in the hGSTM1a−GS-DNB complex (bond angles, interatomic distances, and improper angles) is similar to that reported for the GS-DNB complex with rGSTM1-1 (Figures 2 and 4A). Superimposi-

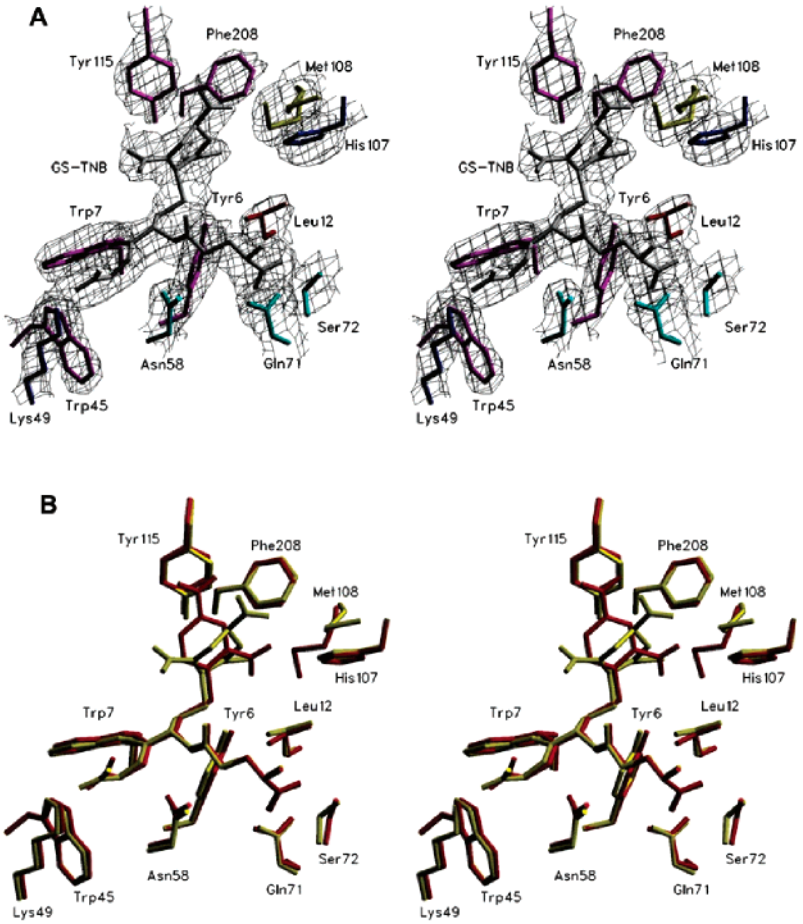

FIGURE 3: Structure of the hGSTM1a complexed with 1-*S*-(glutathionyl)-2,4,6-trinitrocyclohexadienate. (A) Stereoview of the 2Fo-Fc map (sigma level cut off was 0.8) drawn around the residues of the catalytic site of human GSTM1a-1a complexed with 1-*S*-(glutathionyl)-2,4,6-trinitrocyclohexadienate (GS-TNB) (pdb 2F3M). The trinitrocyclohexadienate moiety was omitted from map calculations. (B) Stereoview of the superimposition of active-site residues taken from the coordinates of hGSTM1a-1a complexed with GS-DNB (pdb 1WXK, red) and 1-*S*-(glutathionyl)-2,4,6-trinitrocyclohexadienate (pdb 2F3M, yellow). The coordinates for the monomer A were used in each case.

tion of the coordinates of the hGSTM1a-1a−GS-DNB complex with the coordinates for other similar complexes obtained for rGSTM1-1 product complexes, however, shows differences in orientation of their DNB rings in the protein (Figure 4A). For instance, the DNB ring of the rGSTM1−GS-DNB complex is oriented out of the active site pocket of the enzyme and was observed in two alternate (flip-flop) conformations within the same GST homodimer in the asymmetric unit. The only possible contact between the DNB ring and the protein in that structure is between the ortho nitro group and the sulfur atom of the Met108 side chain. The same contact was also observed in the hGSTM2-2−GS-DNB complex (*25*) in which the DNB ring is not entirely resolved in ED maps, suggesting a high degree of flexibility of this part of the product.

Ji et al. (*40*) crystallized rGSTM1-1 in the presence of a putative transition state analogue, which is a product of the reaction between 1,3,5-trinitrobenzene (1,3,5-TNB) and GSH. In that structure, the TNB ring adopted a conformation that is quite different from that of the DNB ring of the GS-DNB−enzyme complex suggesting that the configuration of the DNB ring of the product is different from that of the transition state complex. Structures of human hGSTM1a-1a (pdb 2F3M) and rat rGSTM1-1 (pdb 4GST) complexed with 1-*S*-(glutathionyl)-2,4,6-trinitrocyclohexadienate show clear differences in the orientation of their trinitrocyclohexadienate rings, even though their GSH moieties retain very similar conformations (Figure 4B). It is noteworthy however that one of the 2-nitro groups of the trinitrocyclohexadienate moiety in both structures can be hydrogen bonded to the hydroxyl groups of Tyr115 and/or Tyr6 (the 2-nitro group for the human enzyme−ligand complex and the 6-nitro group for the rat rGSTM1-1 complex). The structure is consistent with the involvement of both Tyr6 and Tyr115 in catalysis via transition-state stabilization for both enzymes (see discussion below).

Kinetic Studies with hGSTM1a-1a Active-Site Mutants. The second-order rate constants for the nucleophilic addition or substitution reactions between GSH and electrophilic substrates are pH dependent, reflecting concentrations of the GSH thiolate anion (GS^-) in solution, which in turn, depends on the pK_a of the thiol group of GSH in solution (about 8.7 for nonenzymatic reactions). Maximal values of rate constants for nonenzymatic reactions between aryl halogenenated compounds and GSH are achieved at pH values of about 9.0. The rate constant of the noncatalyzed reaction between FDNB and GSH (k_1 ~140 $M^{-1}s^{-1}$) is more than 50-fold greater than that for CDNB (k_1 ~2.7 $M^{-1}s^{-1}$).

The amino acid side chains of Tyr6, Leu12, His107, Met108, and Tyr115 are in close proximity to the DNB ring of GS-DNB in the active site of hGSTM1a-1a (Figure 3) and were targeted for kinetic studies with minimal disruption

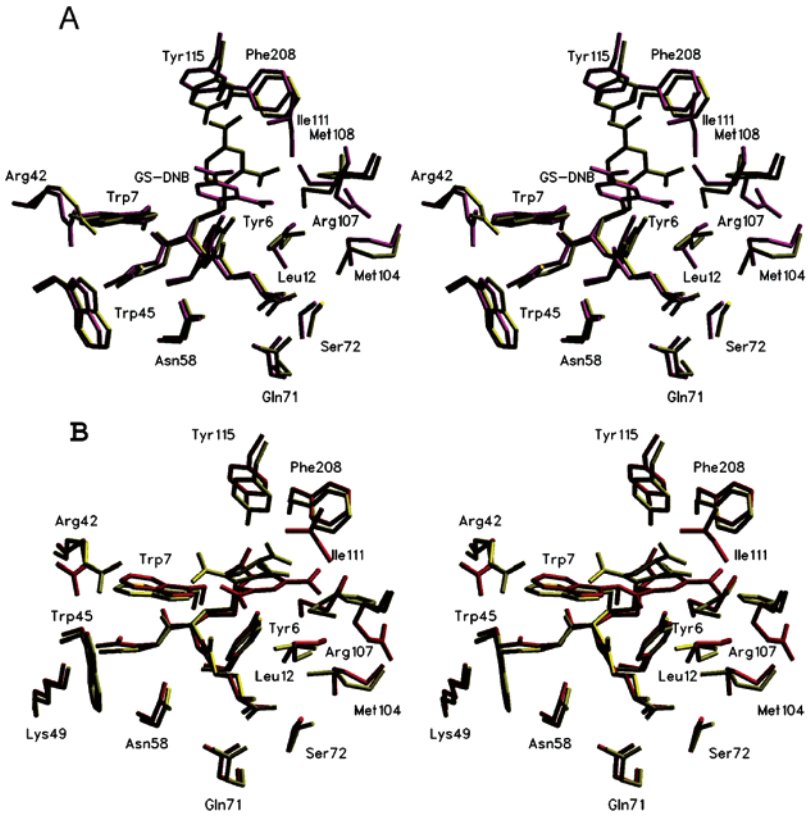

FIGURE 4: Comparison of active sites of human GSTM1a-1a and rat GSTM1-1. (A) Stereoview of the superimposition of active-site residues taken from the coordinates of human GSTM1a-1a (pdb 1WXK, yellow) and rat GSTM1-1 (pdb 5GST, red) both complexed with GS-DNB. Note the different orientations of the DNB rings. (B) Stereoview of the superimposition of active-site residues taken from coordinates of hGSTM1a-1a (pdb 2F3M, yellow) rat GSTM1-1 (pdb 4GST, red) both complexed with 1-*S*-(glutathionyl)-2,4,6-trinitrocyclohexadienate. The coordinates for monomer A were used in each case.

Table 1: Kinetic Parameters of hGSTM1a-1a Active-Site Mutants with CDNB and FDNB as Second Substrates[a]

mutation	substrate	k_{cat} (s^{-1})	$K_m^{(GSH)}$ (mM)	$K_m^{(SS)b}$ (mM)	K_{cat}/K_m(GSH)	$K_{cat}/K_m^{(SS)}$ (s^{-1} m M^{-1})	pK_a[c]
wild-type	CDNB	72.0 ± 11.2	0.14 ± 0.03	0.39 ± 0.06	514	185	6.2 ± 0.2
	FDNB	21.0 ± 4.3	0.12 + 0.02	0.02 ± 0.01	175	1050	6.4 ± 0.2
Y6F	CDNB	0.8 ± 0.3	0.15 + 0.06	0.27 ± 0.12	5.3	3	6.5 ± 0.3
Y6F	FDNB	0.3 ± 0.2	0.14 + 0.05	0.025 ± 0.014	2.1	12	6.4 ± 0.4
Y115F	CDNB	102 ± 20.4	0.12 + 0.03	0.29 ± 0.07	850	352	6.2 ± 0.2
	FDNB	120 ± 13.2	0.11 + 0.02	0.13 ± 0.04	1091	953	6.3 ± 0.3
Y115A	CDNB	6.5 ± 1.4	0.21 + 0.065	1.65 ± 0.55	31	4	6.3 ± 0.3
	FDNB	5.3 ± 2.3	0.17 + 0.04	0.41 ± 0.08	31	13	6.2 ± 0.4
L12V	CDNB	31.0 ± 6.4	0.39 + 0.11	0.40 ± 0.09	80	76	6.3 ± 0.3
	FDNB	26.0 ± 4.3	0.37 + 0.07	0.038 ± 0.014	73	675	6.3 ± 0.2
H107Q	CDNB	27.0 ± 4.8	0.17 + 0.04	0.78 ± 0.24	159	35	7.8 ± 0.4
	FDNB	32.0 ± 6.3	0.14 + 0.03	0.035 ± 0.011	229	914	7.8 ± 0.6
M108I	CDNB	38.0 ± 5.5	0.38 + 0.13	0.84 ± 0.24	100	42	6.2 ± 0.3
	FDNB	18.0 ± 4.7	0.40 + 0.15	0.055 ± 0.017	45	327	6.2 ± 0.3
M104I	CDNB	32.0 ± 7.4	0.45 + 0.14	0.76 ± 0.23	71	42	6.3 ± 0.3
	FDNB	12.0 ± 4.1	0.41 + 0.17	0.046 ± 0.013	30	261	6.4 ± 0.3

[a] The limiting values of kinetic constants are shown. [b] $K_m^{(SS)}$ is the K_m value for the indicated second substrate. [c] The pK_a value for k_{cat} in pH units.

of hydrogen bond and solvent networks. On that basis Tyr6Phe, Tyr115Phe, Tyr115Ala, Leu12Val, His107Gln, and Met108Ile mutants were prepared. For the wild-type enzyme and all of the hGSTM1a-1a mutants, catalytic pK_a values and limiting values of kinetic constants using CDNB and FDNB as second substrates were measured (Table 1). With both CDNB and FDNB as substrates, the catalytic pK_a values for most of the mutants remained between 6.2 and 6.5, with the exception of the His107Gln substitution (pK_a is close to 8.0). These results underscore the importance of His107 in catalysis at more acidic pH values and are consistent with previous suggestions (*22*). As expected, most of the substitutions did not affect the apparent affinity of the enzyme for GSH; $K_m^{(GSH)}$ values were between 0.1 and 0.2 mM, with both FDNB and CDNB as second substrates (except for a modest 2-fold decrease in affinity for the Leu12Val and Met108Ile mutants ($K_m^{(GSH)}$ about 0.4 mM). In contrast, the substitutions affected catalytic efficiencies either because of

the changes in K_m values for the second substrates or by changes in turnover number. For the wild-type enzyme, the $K_m^{(CDNB)}$ (0.39 mM) value is far greater than the $K_m^{(FDNB)}$ value (0.02 mM). The $k_{cat}^{(CDNB)}$ value however, is more than 3 times greater than $k_{cat}^{(FDNB)}$, even though FDNB is a more reactive compound. The transition state itself is probably similar for both substrates (CDNB and FDNB). In that case, amino acid substitutions that affect FDNB binding but do not affect the stability of the tetrahedral transition state should increase the turnover numbers. Conversely, mutations that increase substrate affinity should lower the k_{cat} values. On the basis of K_m values, CDNB as a second substrate apparently binds with a lower affinity than does FDNB, and all of the amino acid substitutions tested had relatively small effects on $K_m^{(CDNB)}$ values. The Met108Ile and His107Gln substitutions increased the $K_m^{(CDNB)}$ value from 0.39 (wild-type) to 0.8 mM. The Tyr115Ala substitution increased $K_m^{(CDNB)}$ to 1.65 mM. The Tyr6Phe, Leu12Val substitutions had no significant effect on $K_m^{(CDNB)}$. In contrast, these mutations caused substantial changes in turnover numbers. Thus, the Tyr6Phe mutant retained less than 1% of the wild-type activity, and the Tyr115Ala mutant also lost about 90% of the enzymatic activity. The His107Gln, Met108Ile, and Leu12Val mutants each retained about half of the wild-type activity (Table 1). The Tyr115Phe substitution however, increased the $k_{cat}^{(CDNB)}$ value about 2-fold compared to that of the wild-type protein. (Similar results were obtained for a Tyr115Phe mutant of rGSTM1-1 (*39*).)

Because the apparent affinity of FDNB is much greater than that of CDNB as a second substrate, it may be expected that certain mutants exhibit different behaviors with respect to second substrate binding. However, because the transition state is probably the same for both CDNB and FDNB, the mutations within the enzyme active site should have similar effects on k_{cat} values for both substrates even with the different effects on K_m values. For instance, the Tyr115Phe substitution increased $K_m^{(FDNB)}$ and simultaneously elevated $k_{cat}^{(FDNB)}$ values from 21 to about 120 s^{-1}, which is comparable to the $k_{cat}^{(CDNB)}$ value for this mutant (102 s^{-1}). The Tyr115Ala mutation substantially affected $K_m^{(FDNB)}$, which increased from 20 μM (wild-type) to about 0.4 mM (mutant). The $k_{cat}^{(FDNB)}$ value (5.3 s^{-1}) is less affected by this substitution and decreased about 2-fold compared to the $k_{cat}^{(FDNB)}$ value of wild-type hGSTM1a-1a. It is noteworthy, however, that the $k_{cat}^{(FDNB)}$ value for the Tyr115Ala mutant is close to that of $k_{cat}^{(CDNB)}$(5.3 s^{-1}). The His107Gln, Met108Ile, and Leu12Val mutations had relatively small effects on FDNB binding and had little effect on turnover numbers (Table 1). Finally, the Tyr6Phe substitution largely ablates hGSTM1a-1a enzymatic activity with FDNB as a second substrate, even though this mutation has no effect on substrate binding as reflected by the K_m values.

DISCUSSION

Catalysis by GSTs usually involves the activation of enzyme-bound GSH to stabilize a GSH-thiolate anion for reaction with the second substrate (*41*−*43*). The Tyr6 residue of Mu-class GSTs is important for catalysis, and the Tyr6Phe replacement drastically reduces catalytic rates but has no effect on the kinetic pK_a value of hGSTM1a-1a (Table 1), indicating that the proton transfer chain is still operative in the mutant enzyme. GSH bound to the G-site of hGSTM1a-1a is rapidly converted into the GSH-thiolate anion even at pH values below 7.0, and there is a strong correlation between the catalytic pK_a of hGSTM1a-1a (about 6.2) and the pK_a value for the enzyme-bound thiol group of GSH (about 6.5) (*22*). The presence of His107, however, is required for GSH-thiolate anion formation because the replacement of this residue with either Ser, Asn, or Gln sharply increases pK_a values of the mutants (7.8−8.0) as compared to that of the wild-type enzyme (6.2) (Table 1) (*22*). In contrast, the same substitutions have much smaller effects on K_m values and turnover numbers in the enzymatic reactions (Table 1). Most other known human and rodent Mu-class GSTs have an Arg107 residue; human hGSTM1 and hGSTM5 are the only known subunits with histidine at that position. His107 probably functions as a proton acceptor/electron donor in the first step of catalysis (*22*). The crystal structure of the hGSTM1a−GSH complex (Figure 1) suggests that a proton can be transferred between GSH and the His107 side chain by means of two tightly bound water molecules (designated WAT1 and WAT2 in Figure 1).

Predictions based on the crystal structures of the complexes with GSH derivatives in this study and ligand-free Mu-class GSTs (pdb 1GTU, 2GTU, 3GTU, 4GTU) are consistent with the notion that the G-site topologies of these enzymes are conserved. Although CDNB is not a natural substrate, it is widely used to measure overall activities in cell extracts and to characterize specific GSTs (*31*). CDNB also is used to study the properties of H-sites of GSTs and to determine catalytic mechanisms. The structure of the GS-DNB complexed with hGSTM1a-1a (Figure 2) shows that the product of conjugation can actually resemble the transition state more closely than previously thought (Figure 3B). According to the kinetic and crystallographic data presented here, the second substrate-binding site (H-site) includes the side chains of Leu12, His107, Met108, and Tyr115; the replacement of each of those residues changes the K_m values for CDNB and FDNB. The Tyr6 hydroxyl group is probably not directly involved in binding these substrates because the Tyr6Phe substitution does not affect their K_m values even though the k_{cat} values are greatly reduced. The relative orientation of the DNB ring of CDNB or FDNB bound at the active site is determined by interactions with the Tyr115 and the Met108 side chains. Polar interactions between the ortho nitro group of CDNB/FDNB and the His107 and Met108 (sulfur atom) side chains probably direct the halogen atom of the substrate closer to the thiol group of bound GSH. It is possible, however, for the second substrate to be bound to the H-site in two different orientations depending on whether the ortho or para nitro group interacts with the His107 and Met108 side chains. (These may be called productive or nonproductive binding modes, respectively.) Although the latter possibility cannot be ruled out, the kinetic data in Table 1 indicates that the nature of the halogen atom is important for the binding of the second substrate, thereby promoting the productive binding mode. For instance, the Tyr115Phe replacement increases the $K_m^{(FDNB)}$ value, suggesting that the Tyr115 hydroxyl group (or possibly WAT1, which is hydrogen bonded to the Tyr115 side chain) is a most likely participant in polar interactions with the ortho nitro groups of the substrates. Because the fluorine atom is smaller than chlorine, contacts involving FDNB can allow for the proper orientation of the ortho nitro group with Tyr115 to promote

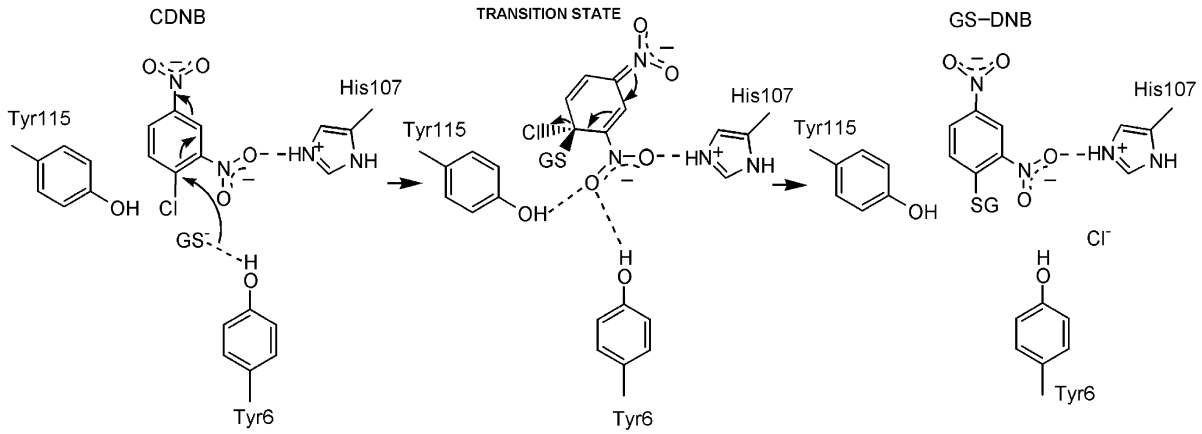

FIGURE 5: Proposed catalytic mechanism for human GSTM1a-1a. Involvement of Tyr6, His107, and Tyr115 at the active site are shown. Note the participation of Tyr6 in the transition-state complex formation.

binding. This is consistent with the observed higher apparent affinity of FDNB compared to that of CDNB (Table 1). On the basis of the kinetics of the amide proton exchange, it was suggested that the Tyr115Phe mutation increases segmental motion in this region to enhance the rate of product release in the case of the rat enzyme rGSTM1-1 (*44*). For hGSTM1a-1a, however, the crystallographic and catalytic evidence cited below is consistent with an alternative explanation to account for the increases of both k_{cat} and K_m values for the Tyr115 mutants.

Binding of a second aromatic substrate disrupts the proton transfer chain in the hGSTM1a-1a active site so that the GSH thiolate anion can only then be stabilized via interactions with the Tyr6 hydroxyl group. The structural data suggests that in the ternary enzyme−substrate complex the thiolate anion is no longer accessible to solvent (water) molecules that may serve as proton donor groups; therefore, the GSH-thiolate anion once formed remains unaffected by the binding of a hydrophobic second substrate. In addition, because the rate of proton exchange is usually much greater ($\sim 10^{11}$ $M^{-1}s^{-1}$) than any other step of enzymatic catalysis, thiolate anion formation cannot be greatly affected by the binding of CDNB or FDNB. This notion is consistent with the kinetic data demonstrating that catalytic pK_a values are identical for CDNB and FDNB (Table 1) as well as for other much less reactive compounds such as 1-chloro-3,4-dinitrobenzene and 1-chloro-2,4-dinitrobenzoic acid (*22*).

As compared to the wild-type enzyme, the Tyr115Ala replacement increases the K_m values for CDNB and FDNB and reduces turnover numbers, suggesting that Tyr115 is involved in both the binding of second substrates and the chemical step of catalysis. The decrease in catalytic efficiency (Table 1) accounts for about 1.5−2 kcal/mol of overall energy loss in catalysis for the Tyr115Ala mutant as compared to that for the wild-type enzyme. The importance of hydrophobic interactions between the Tyr115 and the DNB aromatic rings is evident from the Tyr115Phe substitution, which increases K_m and k_{cat} values. The His107Ser replacement increases the K_m values for CDNB and FDNB (data not shown) and reduces the k_{cat} values for these substrates as compared to that in the wild-type enzyme, suggesting the involvement of His107 in the binding of second substrates as well as in the chemical step of catalysis. The same substitution also increases the catalytic pK_a from 6.2 (wild-type) to about 7.8 (mutant) (*22*). In contrast, the His107Asn substitution only increases the catalytic pK_a but does not change limiting values for K_m and k_{cat} (*22*), suggesting that Asn107, which has a longer side chain than Ser107, substitutes for His107 in substrate binding and in transition-state stabilization. However, the His107Asn mutant cannot stabilize the thiolate anion at acidic pH values.

The Met108 side chain is involved in the binding of second substrates but is of lesser importance for the chemical step of catalysis because the Met108Ala substitution mainly affects the K_m values for CDNB and FDNB (Table 1). Leu12, which is located close to the Tyr6, His107, and Met108 side chains, is not directly involved in substrate binding, but it is important for the structural integrity of the H- and G-sites. The Leu12Val replacement has a little effect on catalysis; however, the Leu12Ile replacement reduces the k_{cat} values, thus suggesting that Leu12 is close to the binding site of hGSTM1a-1a (data not shown).

The catalytic mechanism can be deduced from the combined structures of the enzyme complexed with the transition state analogue (Figure 3) and product (Figure 2) and from kinetic data with a series of key active site mutants (Table 1). The structural data and kinetic analyses provide mechanistic evidence in support of a transition state model shown in the scheme in Figure 5. In this model, the protonated His107 imidazole group is hydrogen bonded to the ortho nitro group of CDNB/FDNB, and the halogen atom is located between the Tyr115 and Tyr6 hydroxyl groups. During the chemical step of catalysis, the DNB ring of the substrate moves closer to Tyr115 and is stabilized by hydrophobic interactions with the Tyr115 aromatic group. The ortho nitro group retains its hydrogen bond with His107, and in addition, it forms a hydrogen bond with the Tyr6 and Tyr115 hydroxyl groups. Realignment of the reactive C1 of CDNB or FDNB (electrophilic center) relative to the sulfur atom of GSH occurs for the formation of the transition state (Step 2 in Figure 5). At the same time, the hydrogen bond between the thiol group of GSH and the Tyr6 hydroxyl oxygen is either lost or weakened. In this model, the hydroxyl groups of Tyr6 and/or Tyr115 can interact with the ortho nitro group of the artificial substrate CDNB. The greater k_{cat} values for the Tyr115Phe mutant underscores the adaptable nature of this active site to accommodate different substrates.

FDNB is by far more reactive in non catalyzed reactions; yet, the k_{cat} value for hGSTM1a-1a catalysis is, surprisingly, more than 3- times less than that for CDNB (Table 1).

Although the products for GST catalyzed reactions with CDNB and FDNB are the same, the enzymatic reaction rate for the more reactive substrate, FDNB, is slower than that for CDNB. It is also unlikely that product release is rate-limiting on the basis of previous pre-steady-state kinetics and viscosity data (*22*). This observation can thus be explained on the basis of the apparent higher affinities of the enzyme for FDNB (see K_m values in Table 1), which are attained in the ternary enzyme−substrate complex (enzyme−substrate complementarity). The enzymatic reaction rates for these two substrates are the result of the formation of the same or very similar transition states that are determined by the structure of the enzyme active site. Accordingly, it is reasonable to presume that the formation of the transition state can be rate limiting, whether or not it involves a conformational transition preceding product release or accompanying substrate recharging.

ACKNOWLEDGMENT

We thank Dr. Vern L. Schramm for his valuable suggestions and critical review of this manuscript.

REFERENCES

1. Jakoby, W. B. (1978) The glutathione S-transferases: a group of multifunctional detoxification proteins, *Adv. Enzymol. Relat. Areas Mol. Biol. 46*, 383−414.
2. Mannervik, B. (1985) The isoenzymes of glutathione transferase, *Adv. Enzymol. Relat. Areas Mol. Biol. 57*, 357−417.
3. Mannervik, B., and Danielson, U. H. (1988) Glutathione transferases−structure and catalytic activity, *Crit. Rev. Biochem. 23*, 283−337.
4. Jakoby, W. B., and Ziegler, D. M. (1990) The enzymes of detoxication, *J. Biol. Chem. 265*, 20715−20718.
5. Rushmore, T. H., and Pickett, C. B. (1993) Glutathione S-transferases, structure, regulation, and therapeutic implications, *J. Biol. Chem. 268*, 11475−11478.
6. Ketterer, B., and Christodoulides, L. G. (1994) Enzymology of cytosolic glutathione S-transferases, *Adv. Pharmacol. 27*, 37−69.
7. Hayes, J. D., and Pulford, D. J. (1995) The glutathione S-transferase supergene family: regulation of GST and the contribution of the isoenzymes to cancer chemoprotection and drug resistance, *Crit. Rev. Biochem. Mol. Biol. 30*, 445−600.
8. Armstrong, R. N. (1997) Structure, catalytic mechanism, and evolution of the glutathione transferases, *Chem. Res. Toxicol. 10*, 2−18.
9. Coles, B. F., and Kadlubar, F. F. (2003) Detoxification of electrophilic compounds by glutathione S-transferase catalysis: determinants of individual response to chemical carcinogens and chemotherapeutic drugs? *Biofactors 17*, 115−130.
10. Hayes, J. D., Flanagan, J. U., and Jowsey, I. R. (2005) Glutathione transferases, *Annu. Rev. Pharmacol. Toxicol. 45*, 51−88.
11. Pickett, C. B. (1987) Structure and regulation of glutathione S-transferase genes, *Essays Biochem. 23*, 116−143.
12. Tetlow, N., Robinson, A., Mantle, T., and Board, P. (2004) Polymorphism of human mu class glutathione transferases, *Pharmacogenetics 14*, 359−368.
13. Daniel, V. (1993) Glutathione S-transferases: gene structure and regulation of expression, *Crit. Rev. Biochem. Mol. Biol. 28*, 173−207.
14. Mannervik, B., Alin, P., Guthenberg, C., Jensson, H., Tahir, M. K., Warholm, M., and Jornvall, H. (1985) Identification of three classes of cytosolic glutathione transferase common to several mammalian species: correlation between structural data and enzymatic properties, *Proc. Natl. Acad. Sci. U.S.A. 82*, 7202−7206.
15. Mannervik, B., Awasthi, Y. C., Board, P. G., Hayes, J. D., Di Ilio, C., Ketterer, B., Listowsky, I., Morgenstern, R., Muramatsu, M., Pearson, W. R., et al. (1992) Nomenclature for human glutathione transferases, *Biochem. J. 282*, 305−306.
16. Mannervik, B. B., Hayes, P. G., Listowsky, J. D., and Pearson, W. R. (2005) Nomenclature for soluble glutathione transferases, *Methods Enzymol. 401*, 1−8.
17. Seidegard, J., Vorachek, W. R., Pero, R. W., and Pearson, W. R. (1988) Hereditary differences in the expression of the human glutathione transferase active on trans-stilbene oxide are due to a gene deletion, *Proc. Natl. Acad. Sci. U.S.A. 85*, 7293−7297.
18. Pearson, W. R., Vorachek, W. R., Xu, S. J., Berger, R., Hart, I., Vannais, D., and Patterson, D. (1993) Identification of class-mu glutathione transferase genes GSTM1-GSTM5 on human chromosome 1p13, *Am. J. Hum. Genet. 53*, 220−233.
19. Strange, R. C., Spiteri, M. A., Ramachandran, S., and Fryer, A. A. (2001) Glutathione-S-transferase family of enzymes, *Mutat. Res. 482*, 21−6.
20. Townsend, D. M., and Tew, K. D. (2003) The role of glutathione-S-transferase in anti-cancer drug resistance, *Oncogene 22*, 7369−7375.
21. Takahashi, Y., Campbell, E. A., Hirata, Y., Takayama, T., and Listowsky, I. (1993) A basis for differentiating among the multiple human Mu-glutathione S-transferases and molecular cloning of brain GSTM5, *J. Biol. Chem. 268*, 8893−8898.
22. Patskovsky, Y. V., Patskovska, L. N., and Listowsky, I. (1999) Functions of His107 in the catalytic mechanism of human glutathione S-transferase hGSTM1a-1a, *Biochemistry 38*, 1193−1202.
23. Patskovsky, Y. V., Patskovska, L. N., and Listowsky, I. (2000) The enhanced affinity for thiolate anion and activation of enzyme-bound glutathione is governed by an arginine residue of human Mu class glutathione S-transferases, *J. Biol. Chem. 275*, 3296−3304.
24. Ji, X., Zhang, P., Armstrong, R. N., and Gilliland, G. L. (1992) The three-dimensional structure of a glutathione S-transferase from the mu gene class. Structural analysis of the binary complex of isoenzyme 3-3 and glutathione at 2.2-A resolution, *Biochemistry 31*, 10169−10184.
25. McCallum, S. A., Hitchens, T. K., Torborg, C., and Rule, G. S. (2000) Ligand-induced changes in the structure and dynamics of a human class Mu glutathione S-transferase, *Biochemistry 39*, 7343−7356.
26. Raghunathan, S., Chandross, R. J., Kretsinger, R. H., Allison, T. J., Penington, C. J., and Rule, G. S. (1994) Crystal structure of human class mu glutathione transferase GSTM2-2. Effects of lattice packing on conformational heterogeneity, *J. Mol. Biol. 238*, 815−832.
27. Ji, X., Tordova, M., O'Donnell, R., Parsons, J. F., Hayden, J. B., Gilliland, G. L., and Zimniak, P. (1997) Structure and function of the xenobiotic substrate-binding site and location of a potential nonsubstrate-binding site in a class pi glutathione S-transferase, *Biochemistry 36*, 9690−9702.
28. Oakley, A. J., Lo Bello, M., Nuccetelli, M., Mazzetti, A. P., and Parker, M. W. (1999) The ligandin (nonsubstrate) binding site of human Pi class glutathione transferase is located in the electrophile binding site (H-site), *J. Mol. Biol. 291*, 913−926.
29. Wilce, M. C., and Parker, M. W. (1994) Structure and function of glutathione S-transferases, *Biochim. Biophys. Acta. 1205*, 1−18.
30. Rowe, J. D., Nieves, E., and Listowsky, I. (1997) Subunit diversity and tissue distribution of human glutathione S-transferases: interpretations based on electrospray ionization-MS and peptide sequence-specific antisera, *Biochem. J. 325*, 481−486.
31. Habig, W. H., and Jakoby, W. B. (1981) Assays for differentiation of glutathione S-transferases, *Methods Enzymol. 77*, 398−405.
32. Rietjens, I. M., Soffers, A. E., Hooiveld, G. J., Veeger, C., and Vervoort, J. (1995) Quantitative structure−activity relationships based on computer calculated parameters for the overall rate of glutathione S-transferase catalyzed conjugation of a series of fluoronitrobenzenes, *Chem. Res. Toxicol. 8*, 481−488.
33. Soffers, A. E., Ploemen, J. H., Moonen, M. J., Wobbes, T., van Ommen, B., Vervoort, J., van Bladeren, P. J., and Rietjens, I. M. (1996) Regioselectivity and quantitative structure−activity relationships for the conjugation of a series of fluoronitrobenzenes by purified glutathione S-transferase enzymes from rat and man, *Chem. Res. Toxicol. 9*, 638−646.
34. Brunger, A. T. (1992) *X-PLOR. A System for X-ray Crystallography and NMR*, Yale University Press, New Haven, CT.
35. Brunger, A. T., Adams, P. D., Clore, G. M., DeLano, W. L., Gros, P., Grosse-Kunstleve, R. W., Jiang, J. S., Kuszewski, J., Nilges, M., Pannu N. S., Read, R. J., Rice, L. M., Simonson, T., Warren, G. L. (1998) Crystallography & NMR system: A new software

suite for macromolecular structure determination, *Acta Crystallogr., Sect. D 54*, 905−921.
36. Kleywegt, G. J. (1995) Dictionaries for Heteros. CCP4/ESF, *CCP4/ESF-EACBM Newsl. Protein Crystallogr. 31*, 45−50.
37. Laskowski, R. A., MacArthur, M. W., Moss, D. S., and Thornton, J. M. (1993) PROCHECK: a program to check the stereochemical quality of protein structures, *J. Appl. Crystallogr. 26*, 283−291.
38. Ji, X., Johnson, W. W., Sesay, M. A., Dickert, L., Prasad, S. M., Ammon, H. L., Armstrong, R. N., and Gilliland, G. L. (1994) Structure and function of the xenobiotic substrate binding site of a glutathione *S*-transferase as revealed by X-ray crystallographic analysis of product complexes with the diastereomers of 9-(*S*-glutathionyl)-10-hydroxy-9, 10-dihydrophenanthrene, *Biochemistry 33*, 1043−1052.
39. Johnson, W. W., Liu, S., Ji, X., Gilliland, G. L., and Armstrong, R. N. (1993) Tyrosine 115 participates both in chemical and physical steps of the catalytic mechanism of a glutathione S-transferase, *J. Biol. Chem. 268*, 11508−11511.
40. Ji, X., Armstrong, R. N., and Gilliland, G. L. (1993) Snapshots along the reaction coordinate of an SNAr reaction catalyzed by glutathione transferase, *Biochemistry 32*, 12949−12954.
41. Graminski, G. F., Zhang, P. H., Sesay, M. A., Ammon, H. L., and Armstrong, R. N. (1989) Formation of the 1-(S-glutathionyl)-2,4,6-trinitrocyclohexadienate anion at the active site of glutathione S-transferase: evidence for enzymic stabilization of sigma-complex intermediates in nucleophilic aromatic substitution reactions, *Biochemistry 28*, 6252−6258.
42. Liu, S., Zhang, P., Ji, X., Johnson, W. W., Gilliland, G. L., and Armstrong, R. N. (1992) Contribution of tyrosine 6 to the catalytic mechanism of isoenzyme 3-3 of glutathione S-transferase, *J. Biol. Chem. 267*, 4296−4299.
43. Caccuri, A. M., Antonini, G., Board, P. G., Parker, M. W., Nicotra, M., Lo Bello, M., Federici, G., and Ricci, G. (1999) Proton release on binding of glutathione to alpha, Mu and Delta class glutathione transferases, *Biochem. J. 344*, 419−425.
44. Codreanu, S. G., Ladner, J. E., Xiao, G., Stourman, N. V., Hachey, D. L., Gilliland, G. L., and Armstrong, R. N. (2002) Local protein dynamics and catalysis: detection of segmental motion associated with rate-limiting product release by a glutathione transferase, *Biochemistry 41*, 15161−15172.
45. Bico, P., Chen, C. Y., Jones, M., Erhardt, J., and Dirr, H. (1994) Class pi glutathione S-transferase: Meisenheimer complex formation, *Biochem. Mol. Biol. Int. 33*, 887−892.
46. Prade, L., Huber, R., Manoharan, T. H., Fahl, W. E., and Reuter, W. (1997) Structures of class pi glutathione S-transferase from human placenta in complex with substrate, transition-state analogue and inhibitor, *Structure 5*, 1287−1295.

BI051823+